Acta Oceanol. Sin., 2022, Vol. 41, No. 6, P. 99–113
https://doi.org/10.1007/s13131-021-1934-8
http://www.aosocean.com
E-mail: ocean2@hyxb.org.cn

Responses of nutrient biogeochemistry and nitrogen cycle to seasonal upwelling in coastal waters of the eastern Hainan Island

Nan Zhou[1, 2], Sumei Liu[1, 2*], Guodong Song[1, 2], Yunyan Zhang[1, 2], Lingyan Wang[1, 2], Xiaoyan Ning[1, 2]

[1] Frontiers Science Center for Deep Ocean Multispheres and Earth System, and Key Laboratory of Marine Chemistry Theory and Technology of Ministry of Education, Ocean University of China, Qingdao 266100, China

[2] Laboratory for Marine Ecology and Environmental Science, Pilot National Laboratory for Marine Science and Technology (Qingdao), Qingdao 266237, China

Received 31 May 2021; accepted 11 October 2021

Abstract

The coastal upwelling has profound influence on the surrounding ecosystem by supplying the nutrient-replete water to the euphotic zone. Nutrient biogeochemistry was investigated in coastal waters of the eastern Hainan Island in summer 2015 and autumn 2016. From perspectives of nutrient dynamics and physical transport, the nutrient fluxes entered the upper 50 m water depth (between the mixed layer and the euphotic zone) arisen from the upwelling were estimated to be 2.5–5.4 mmol/(m^2·d), 0.15–0.28 mmol/(m^2·d), and 2.2–7.2 mmol/(m^2·d) for dissolved inorganic nitrogen (DIN), phosphate (DIP), and dissolved silicate (DSi), respectively, which were around 6- to 12-fold those in the background area. The upwelled nutrients supported an additional plankton growth of (14.70±8.95) mg/m^2 for chlorophyll *a* (Chl *a*). The distributions of nitrate δ^{15}N and δ^{18}O above the 300 m water depth (top of the North Pacific Intermediate Water) were different among the upwelling area, background area in summer, and the stations in autumn, and the difference of environmental and biogeochemical conditions between seasons should be the reason. The higher DIN/DIP concentration ratio, nitrate concentration anomaly, and lower nitrate isotope anomaly (Δ(15, 18)) in the upper ocean in summer than in autumn indicated the stronger nitrogen fixation and atmospheric deposition, and the following fixed nitrogen regeneration in summer. The higher values of Chl *a* and nitrate δ^{15}N and δ^{18}O within the euphotic zone in autumn than the background area in summer suggested the stronger nitrate assimilation in autumn. The differences in relatively strength of the assimilation, nitrogen fixation and atmospheric deposition, and the following remineralization and nitrification between the two seasons made the higher δ^{18}O:δ^{15}N and larger difference of enzymatic isotope fractionation factors $^{15}\varepsilon$ and $^{18}\varepsilon$ for nitrate assimilation in summer than in autumn above the North Pacific Tropical Water.

Key words: nutrients, upwelling, nitrate δ^{15}N and δ^{18}O, nitrogen cycle, South China Sea

Citation: Zhou Nan, Liu Sumei, Song Guodong, Zhang Yunyan, Wang Lingyan, Ning Xiaoyan. 2022. Responses of nutrient biogeochemistry and nitrogen cycle to seasonal upwelling in coastal waters of the eastern Hainan Island. Acta Oceanologica Sinica, 41(6): 99–113, doi: 10.1007/s13131-021-1934-8

1 Introduction

The upwelling is an important physical process as it can bring cold, nutrient-replete water to the euphotic zone to support the growth of primary producers, which plays a significant role in the biogeochemistry, primary production, and fisheries in the marine ecosystem (Hu and Wang, 2016; McGregor et al., 2007; Pauly and Christensen, 1995). The Ekman transport and Ekman pumping induced by wind combined with the bottom topography and tidal mixing make the marginal seas be the hot place for upwellings (Lin et al., 2016; Su and Pohlmann, 2009; Wang et al., 2013, 2015). The area of the coastal upwelling occupies only 1% of the global oceans, but contributes more than 10% of the new production and 20% of the fisheries in the world oceans (Chavez and Toggweiler, 1995; Pauly and Christensen, 1995). The Chinese marginal seas are abundant with coastal upwelling systems and more than half of them are in the South China Sea (SCS) (Hu and Wang, 2016).

The Hainan Island is situated in the southern part of China in the SCS with the surface area of 3.54×10^4 km^2 and is dominated by the tropical maritime monsoon climate with southwesterly monsoon in summer and northeasterly monsoon in winter. There are dozens of small rivers in the Hainan Island empty into the SCS with a total annual discharge of 3.1×10^{10} m^3 (Zhang et al., 2013), and the annual precipitation is 1 500 mm to 2 000 mm. More than 80% of the riverine discharge and rainfall is in the wet season (May to October) (Herbeck et al., 2020; Li et al., 2013, 2014; Liu et al., 2011; Zhang et al., 2006). The coast of the Hainan Island with the coastline length of 1 550 km has various biological habitat types including mangroves, coral reefs, and lagoons (Li et al., 2014). The seasonal upwelling in coastal waters of the eastern Hainan Island (EHI) is one of the most famous coastal upwelling systems in the SCS and has been studied since the 1960s (Guan and Chen, 1964). Generally, the upwelling starts in April, develops to the peak period during June and July, dissipates in September, and locates at the area between 18.5°N to 20°N and west of 111.5°E, and the upward speed is in the order of 10 $^{-5}$ m/s

Foundation item: The National Natural Science Foundation of China under contract No. 41376086; the Taishan Scholars Programme of Shandong Province; the Aoshan Talents Program supported by the Pilot National Laboratory for Marine Science and Technology (Qingdao) under contract No. 2015ASTP-OS08.

*Corresponding author, E-mail: sumeiliu@ouc.edu.cn

(Chai et al., 2001; Deng et al., 1995; Jing et al., 2009; Su et al., 2011b). The coastal upwelling system of the EHI varies interannually because of being affected by multiple environmental factors (e.g., East Asian summer monsoon, ENSO, rainfall, and tide) (Jing et al., 2011; Liu et al., 2013; Wang et al., 2015).

Nutrients are the essential, and usually, the limiting elements for the growth and reproduction of marine primary producers. Nitrogen cycle is a hot and difficult topic in the nutrient biogeochemical studies because of its multiple cycling processes and directly coupling with other biogenic elements (e.g., C, P and Si) through biological activities. The nitrate dual isotopes provide a powerful tool to constrain nitrogen cycle because of the characteristic $\delta^{15}N$ and $\delta^{18}O$ values (the computing method of $\delta^{15}N$ (‰) or $\delta^{18}O$ (‰) is $(R_{sample}/R_{standard}-1)\times 1\,000$, referenced to air N_2 or the Vienna Standard Mean Ocean Water, where R is concentration ratio of $^{15}N/^{14}N$ or $^{18}O/^{16}O$) of various nitrate sources; and the different enzymatic isotope fractionation factor (ε, $^{15}\varepsilon$ (‰)= $[(^{14}k/^{15}k)-1]\times 1\,000$, where ^{14}k and ^{15}k represent the rate constants for the light and heavy N isotopes, respectively, and similarly for $^{18}\varepsilon$ with respect to O) among different nitrogen cycling processes. For example, the $\delta^{15}N$ of new fixed N introduced from marine nitrogen fixation is approximately –1‰±1‰ (Hoering and Ford, 1960); the ε of nitrate assimilation is obviously lower than that of denitrification in water column (~5‰ vs. ~20‰; Granger et al., 2004, 2008); nitrate assimilation and denitrification in the ocean produce a 1:1 increase in the residual nitrate $\delta^{18}O$ and $\delta^{15}N$, and the coexisting nitrification would result in a higher or lower deviation from this ratio, depending on the initial composition of sinking N (Casciotti et al., 2013; Granger and Wankel, 2016). Besides, nitrogen sources and their relative contribution can be estimated using the isotope balance model (Bourbonnais et al., 2013; Liu et al., 2020b).

The nutrient biogeochemical studies on the upwelling systems in the western SCS are mainly focused on the Vietnamese coast (Bombar et al., 2010; Loick et al., 2007; Voss et al., 2006). For the upwelling system in the coastal EHI, a few studies focusing on the nitrate biogeochemistry and nutrient distributions influenced by the upwelling have been reported (Chai et al., 2001; Han et al., 1990; Zhang et al., 2015; Chen et al., 2020), and the main research works are related to the nutrient budgets in estuaries and lagoons and their nutrient transport to the ocean (Li et al., 2013, 2014; Liu et al., 2011; Su et al., 2011a). However, the seasonal nutrient dynamics, especially, the sources and transfer processes of nitrogen in coastal waters of the EHI under the influence of the seasonal upwelling are still seldom.

As coastal area of the EHI is affected by the strong upwelling in summer, the seasonal nutrient dynamics and nitrogen cycling processes are complicated. Two field observations were carried out in coastal waters of the EHI during the peak and end period of the upwelling in summer 2015 and autumn 2016. With the dataset of hydrological parameters, nutrient concentrations, nitrate nitrogen and oxygen isotopes, chlorophyll *a* (Chl *a*), and dissolved oxygen (DO), we aim to elaborate the importance of nutrients supplied by the upwelling for supporting the primary production within the euphotic zone, and the nitrogen sources as well as the main nitrogen cycling processes in the coastal EHI under influence of the seasonal upwelling in this study.

2 Materials and methods

2.1 *Sampling*

Two field cruises were conducted in coastal area of the EHI on July 1 to 10, 2015 (summer) and September 18 to 20, 2016 (autumn). There were 31 hydrological stations in the summer investigation and 19 of them were collected the biogeochemical samples; and during the autumn investigation, the biogeochemical samples were collected at all the 19 hydrological stations (Fig. 1). A conductivity-temperature-depth (CTD) rosette system (Seabird 911 plus) attached with 5 L Niskin bottles was used to collect discrete water samples from surface to near bottom, and the sampling layers was decided based on *in situ* ecological environment parameters, including temperature, salinity, fluorescence, and DO. When the CTD rosette was settled down on the deck from the water column, silicone tubes were connected to the Niskin bottles; then water samples were collected using glass bottles for DO determination and Nalgene high-density polyethylene (HDPE) bottles for nutrients measurement. Before filtration, part of water sample was stored in Axygen polypropylene tubes for ammonium analysis on board. Then, the rest was filtered through 0.4 μm Whatman Nuclepore polycarbonate membrane (precleaned with 1% HCl and rinsed to neutral with Milli-Q water) using 500 mL Nalgene filtration apparatus. The filter was folded and preserved in aluminum foil and stored at –20°C until being measured the Chl *a* back to laboratory. After

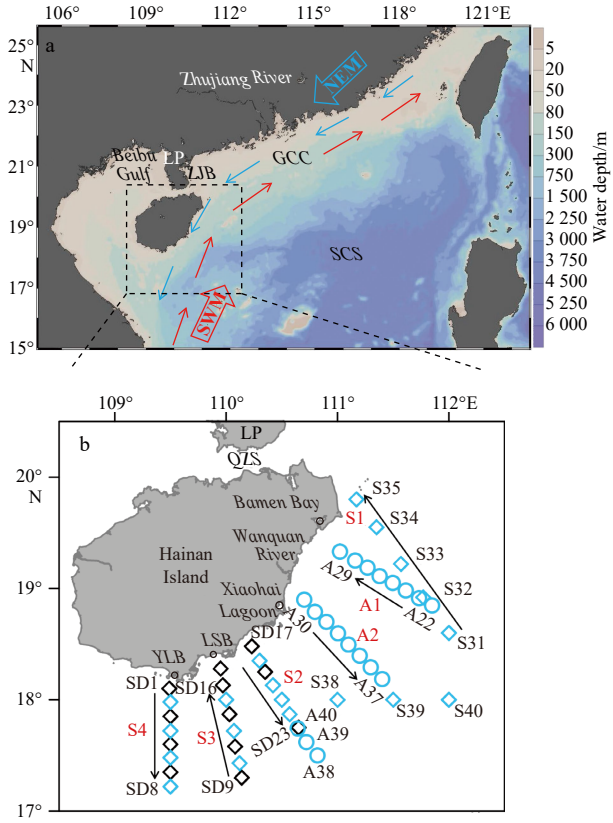

Fig. 1. The study area and sampling stations in coastal waters of the eastern Hainan Island in summer 2015 (rhombuses) and autumn 2016 (circles). The biogeochemical sampling stations were colored as blue, and the black ones were only for hydrological sampling. The directions of monsoon (southwest monsoon, SWM; northeast monsoon, NEM) and Guangdong Coastal Current (GCC) during summer and winter were indicated as red and blue arrows, respectively. Four sections in summer and two sections in autumn were marked from northeast to southwest (S1–S4, A1 and A2 colored as red). SCS is the abbreviation of South China Sea; ZJB, Zhanjiang Bay; LP, Leizhou Peninsula; QZS, Qiongzhou Strait; LSB, Lingshui Bay; YLB, Yulin Bay.

being rinsed three times by the filtrate, two 125 mL Nalgene HDPE bottles were filled with 100 mL filtrate subsamples, the one for analyzing the nitrate nitrogen and oxygen isotopes was added 1 mL 2.5 mmol/L sulfamic acid in 25% HCl to remove nitrite (Weigand et al., 2016) and stored at room temperature; and another one was stored at –20°C for nutrient species analyses. We precleaned the HDPE bottles and filtration apparatuses by soaking them into 10% HCl for three days and rinsing to neutral with deionized water.

2.2 *Measurements of nutrients, DO, and Chl a*

On board, ammonium was analyzed using the fluorometric ortho-phthaldialdehyde method and DO was measured using a DO benchtop meter (JENCO 9173, America) (Kérouel and Aminot, 1997). Nitrate, nitrite, DIP, and DSi were quantified using a QuAAtro autoanalyzer (SEAL Analytical, Germany) back to laboratory. The limitations of detection were 0.02 μmol/L, 0.02 μmol/L, 0.01 μmol/L, 0.01 μmol/L, and 0.03 μmol/L for ammonium, nitrate, nitrite, DIP, and DSi, respectively, and the precision was better than 3%. The total dissolved nitrogen (TDN) and total dissolved phosphorus (TDP) were analyzed using basic-persulfate oxidation (a solution of $K_2S_2O_8$ and H_3BO_3 in NaOH) in an autoclave at 120°C for 30 min to decompose to nitrate and phosphate (Liu et al., 2017). The concentration of dissolved organic nitrogen (DON) and dissolved organic phosphorus (DOP) were calculated from the differences between TDN and DIN (the sum of nitrate, nitrite, and ammonium) and between TDP and DIP. The filter samples for Chl *a* measurement were analyzed by acetone extraction fluorometric determination method (Parsons et al., 1984) with the Chl *a* standard from spinach (Sigma-Aldrich C5753).

2.3 *Nitrate $\delta^{15}N$ and $\delta^{18}O$ analyses*

The water samples for nitrate $\delta^{15}N$ and $\delta^{18}O$ measurement were adjusted the pH to 6–8 by adding 2 mol/L NaOH and analyzed using the denitrifier method (Sigman et al., 2001; Casciotti et al., 2002). In this method, nitrate is converted to N_2O by the denitrifier: *Pseudomonas aureofaciens* which lacks the N_2O reductase. Following, the N_2O was purified and analyzed for the isotopic ratios, *R*, using a purge, cryogenic trap and gas chromatographic separation continuous flow system coupled to an isotope ratio mass spectrometer (IRMS; IsoPrime100, Elementar, Germany). The results were calibrated by the isotope standards: IAEA-N3, USGS34, and USGS35. The $\delta^{15}N$ and $\delta^{18}O$ values of these standards are 4.7‰ and 25.6‰, –1.8‰ and –27.9‰, 2.7‰ and 57.5‰, respectively. An additional lab mixed standard which was made by USGS32 (1 mL, 0.05 mol/L) and USGS34 (10 mL, 0.05 mol/L) was added to calibrate the results to cover all possible $\delta^{15}N$ values of our water samples. The $\delta^{15}N$ value of the lab mixed standard was 14.3‰ that was determined by an elemental analysis IRMS (Vario Micro Cube, Elementar, Germany). The analytical precision was better than 0.2‰ and 0.5‰ for $\delta^{15}N$ and $\delta^{18}O$, respectively.

The isotopic effect of algal nitrate assimilation could be described by the Rayleigh model and depended on whether the nitrate was continuous supplied to the system or not, Rayleigh model was divided to the open system model and closed system model (Liu et al., 2017; Mariotti et al., 1981).

$$\text{Open system}: \delta^{15}N(\delta^{18}O) = \delta^{15}N(\delta^{18}O)_{f=1} + {}^{15}\varepsilon({}^{18}\varepsilon)\times(1-f), \quad (1)$$

$$\text{Closed system}: \delta^{15}N(\delta^{18}O) = \delta^{15}N(\delta^{18}O)_{f=1} - {}^{15}\varepsilon({}^{18}\varepsilon)\ln(f), \quad (2)$$

where *f* was the fraction of unassimilated nitrate in the water column, and ${}^{15}\varepsilon$ (${}^{18}\varepsilon$) was the isotope fractionation factor of nitrogen (oxygen) for nitrate assimilation.

2.4 *Satellite data*

The satellite images of surface seawater potential temperature (SST), surface seawater salinity (SSS), and surface seawater velocity (SSV) were provided by the Copernicus Marine Environment Monitoring Service (http://marine.copernicus.eu/). The reanalysis satellite datasets are the level-4 with spatial and temporal resolutions of (1/12)° and monthly averaged.

2.5 *Statistical analysis*

Statistical analyses were conducted using the SPSS 22 software. The Pearson correlation coefficient was used to determine the correlation between two variables when $p<0.05$. The independent *t*-test was employed to compare the difference between two variables and the difference is significant when $p<0.05$.

3 Results

3.1 *Characteristics of the upwelling*

Indicated from the satellite datasets of SST, SSS, and SSV in the northwestern SCS, performance of the coastal upwelling in the EHI matched evolution of the East Asia monsoon very well (Figs S1 and S2). The sampling of summer 2015 was in the peak period of the upwelling and the sampling period of autumn 2016 was just after the upwelling was dissipated. The difference in distribution of hydrological parameters between summer and autumn was consistent with characteristic driven by this seasonal upwelling (Fig. 2a). In summer, the upwelling brought the cold, salty, and dense deep water to surface and shallowed the mixed layer depth (MLD, which was defined as the water depth that its temperature was 0.5°C lower than that of the surface water; Kara et al., 2000), which made the surface distribution of hydrological parameters display obvious gradient. The nearshore stations had colder and denser surface water as well as shallower MLD than those of the offshore stations, where the differences could reach more than 3°C, 1 kg/m^3, and 20 m, respectively. The salinity of nearshore stations was high in Sections S1 and S2, however, there was a water tongue with slightly lower salinity (around 33.6 to 33.8) from the southwest toward the northeast covered the nearshore stations of Sections S3 and S4, and the middle area of Sections S1 and S2. In contrast, the surface hydrological characteristics were rather constant in autumn.

The temperature, salinity, and density presented an uplifted trend from the offshore toward the nearshore stations in the upper ~150 m in all sections in summer, but the isopleths of hydrological parameters were parallel to the water depth in autumn (Fig. 2b, to reduce the figures, Sections S1 and A1 were shown as the representatives). The temperature-salinity (T-S) diagram was overall in concordance with each other for both seasons and presented the classic "reverse S" shape of the SCS (Fig. 3a), which suggested that though the survey area was not exactly coincident with each other, the water masses were the same. The high salinity water (around 34.6 to 34.7) with the potential density anomaly (σ_0, kg/m^3) from around 24 to 25 indicated the North Pacific Tropical Water (NPTW, around 100–150 m), and the low salinity water (~34.4) with the σ_0 from around 26 to 27 indicated the North Pacific Intermediate Water (NPIW, around 300–700 m) (Liu et al., 1996; Tian et al., 2009). When σ_0 was lower than 25, the water depth presented more related to density in autumn, but it was rather scattered in summer (shallow samples could appear

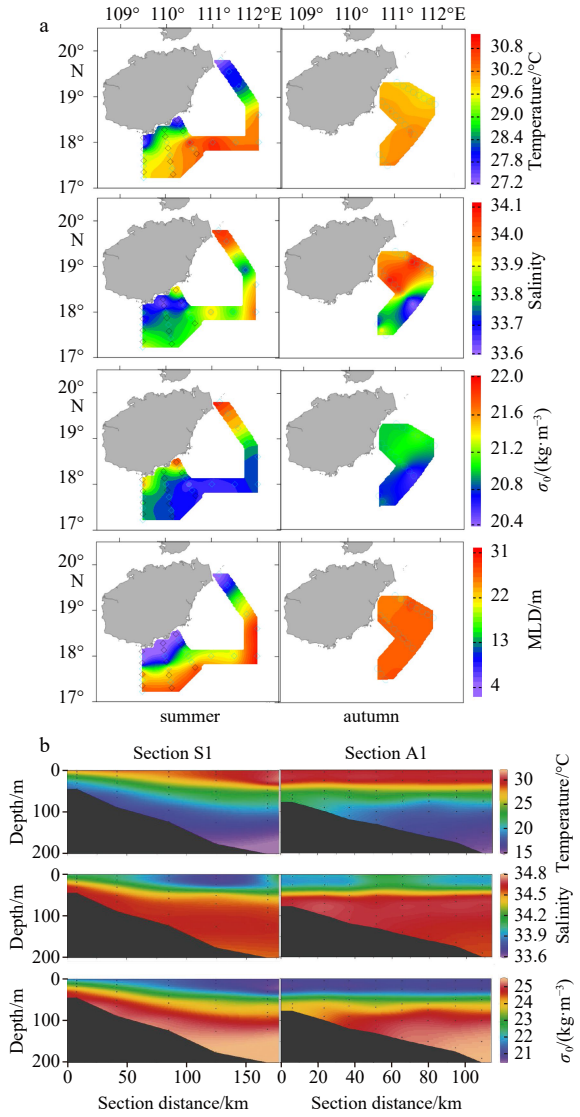

Fig. 2. Surface distribution of temperature, salinity, potential density anomaly (σ_0), and the mixed layer depth (MLD) in coastal waters of the eastern Hainan Island in summer and autumn (a); 200 m water depth sectional distribution of temperature, salinity, and σ_0 in Section S1 in summer and Section A1 in autumn (b).

in high-density area), which was resulted from the nearshore upwelling brought the cold, salty, and dense water to the shallow water depth from below in summer (Fig. 3a). The sampling stations in summer 2015 were divided into nearshore upwelling stations (including Stations SD1 to SD4 in Section S4, Stations SD13 to SD16 in Section S3, Stations SD17 to SD20 in Section S2, and Stations S33 to S35 in Section S1) and offshore stations to illustrate how far the coastal upwelling can extend and how deep it could affect (Fig. 3b). The depth profiles for temperature and density of offshore stations in summer were consistent with the sampling stations in autumn; however, the upwelling stations in summer had obviously lower temperature and higher density above 125 m. Along with the sectional distribution of the hydrological parameters, the nearshore upwelling in summer extended to at least 50 km off the coastline for Sections S2 to S4, and 85 km for Section S1; and it could affect at least 125 m water depth.

3.2 *Nutrients, Chl a, and DO*

3.2.1 *Distribution*

The surface dissolved inorganic nutrients were very low and even below the detection limit (nitrate, nitrite, and DIP) in some regions except for DSi. Ammonium was the main specie of DIN in surface water and the average percentage was 66%±21% in summer and 76%±11% in autumn. The dissolved organic nutrients dominated the total dissolved nutrients at the surface and the percentages of DON and DOP in TDN and TDP were both larger than 90% in two seasons. There were relatively high concentrations of DIN, DIP, DON, DOP, Chl *a*, and DO in coastal upwelling regions of the EHI in summer (Fig. 4). The DSi was higher in the water tongue with slightly lower salinity. In contrast, the surface distribution of biogeochemical parameters was relatively constant in autumn.

The sectional distribution of biogeochemical parameters from offshore toward the nearshore stations in summer and autumn were similar to those of hydrological parameters, which the isopleth presented a tilted-up trend in summer because of the nearshore upwelling, and were parallel with the water depth in autumn (Fig. 5a, to reduce the figures, Sections S1 and A1 were shown as the representatives). Resulted from that the nearshore upwelling supplied the nutrient-replete deep water to the shallower water depth, the DIN, DIP, and DSi of nearshore upwelling stations had higher concentrations in the upper 125 m than those of offshore stations in summer and the stations in autumn (Fig. 5b), even within the nutricline (the water depth that had the biggest increase of nutrient gradient). The depth profiles for DIN, DIP, and DSi of offshore stations in summer and stations in autumn were nearly consistent with each other, which were very low within the nutricline; below the nutricline, concentrations of DIN and DIP increased sharply down to about 500 m, then the increase trend became mildly and were stable at 38 μmol/L to 40 μmol/L and 2.6 μmol/L to 2.9 μmol/L, respectively, below 1 500 m; DSi increased constantly down to about 1 000 m, and the concentration exceeded 150 μmol/L at 2 400 m. DO decreased sharply from the surface to about 500 m, corresponding to the range of water depth for DIN and DIP sharply increased. Then, DO presented the minimum values between around 700 m and 1 000 m at 2.7 mg/L to 3.2 mg/L and increased slightly downward. Nitrite presented a subsurface maximum value in both seasons, which reached 1 μmol/L at the nearshore upwelling stations in summer. The depth of nitrite subsurface maximum values was in concordance with the Chl *a* maximum layer (DCM) for offshore stations in summer and stations in autumn, which was between around 50 m to 100 m. Chl *a* of nearshore upwelling region in the upper 125 m was higher than that of offshore stations in summer (p=0.000, n=41 and n=63 for upwelling and offshore stations, respectively) and stations in autumn (p=0.005, n=41 and n=95 for upwelling stations in summer and stations in autumn, respectively) but scattered. For the offshore stations in summer and stations in autumn, Chl *a* and nitrite in the upper 125 m were significantly higher in autumn (p=0.002 and p=0.01 for Chl *a* and nitrite; n=63 and n=95 for summer and autumn).

3.2.2 *Nutrient ratios*

The slopes of the regression line of DIN to DIP for samples in autumn and offshore stations in summer (Fig. 6) were similar and were consistent with the Redfield ratio (the regression equations were y=15.5x+0.22, r=0.996 and y=15.7x+0.53, r=0.997, respectively). The relationship between DSi and DIN was linear for

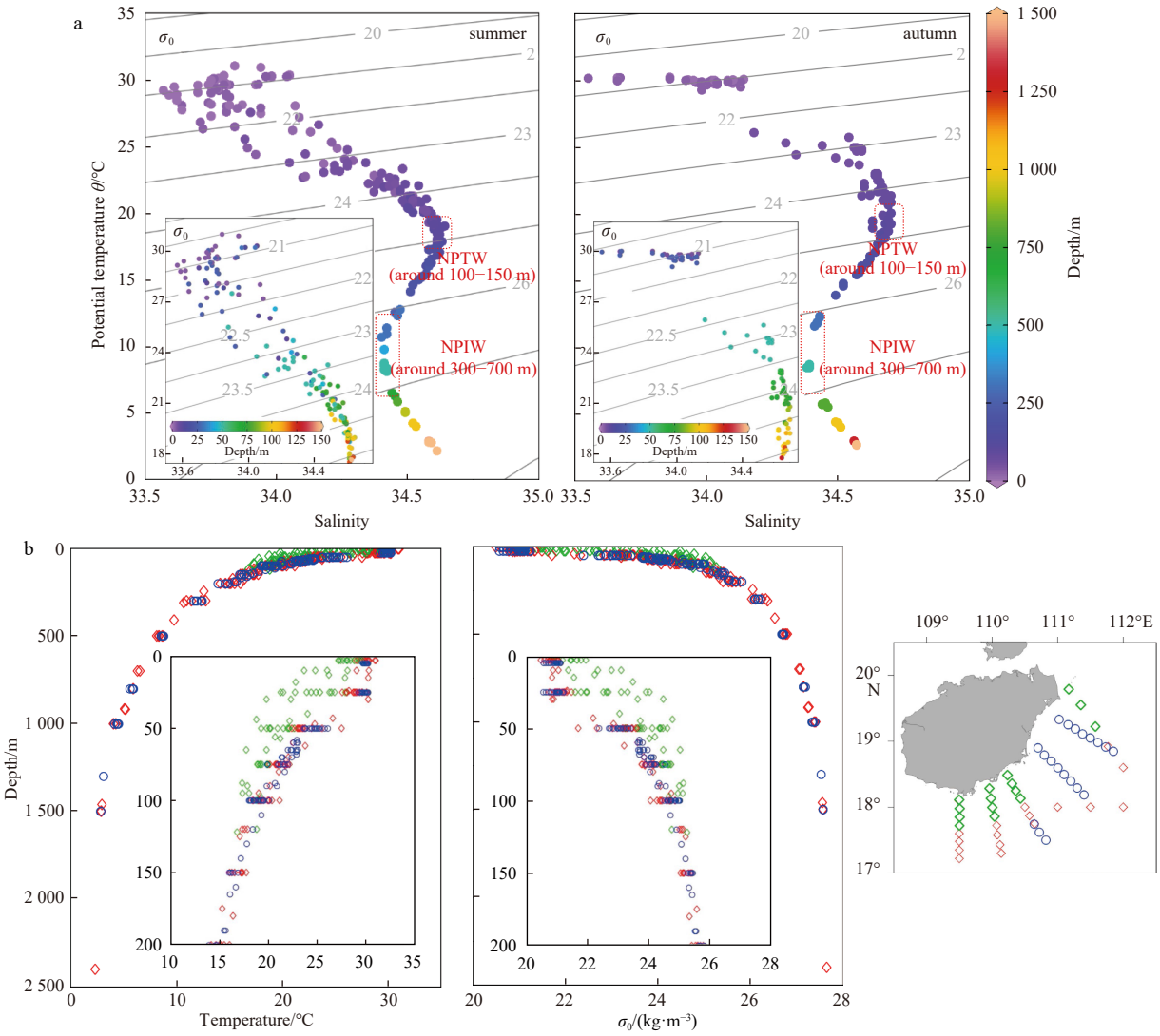

Fig. 3. The temperature–salinity diagram showing isopycnals in coastal waters of the eastern Hainan Island in summer and autumn (a); the color indicated the water depth. The inside figures with smaller ranges of potential temperature, salinity, and water depth (0–150 m) show the details. Depth profiles for temperature and potential density anomaly (σ_0) (b). Dark blue circles were the samples of autumn. Rhombuses were the samples of summer, and green indicated the stations in the nearshore upwelling region and red stood for the offshore background stations. The inside figures were the same as their outside figures only with the water depth above 200 m to show the details. NPTW is the abbreviation of the North Pacific Tropical Water; NPIW, the North Pacific Intermediate Water.

samples above the salinity maximum layer (i.e., NPTW) (k=0.90, r=0.966 for stations in autumn; k=0.81, r=0.971 for offshore stations in summer; k=0.93, r=0.974 for upwelling region in summer, respectively), and the slope of DIN to DIP was higher than that of samples below the NPTW. The slope of DIN to DIP for samples below the NPTW in autumn was similar to that in offshore stations in summer (k=14.0, r=0.994 and k=14.2, r=0.998). However, the slope was significantly higher for samples above the NPTW in summer than those in autumn (k=19.3, r=0.995 for offshore stations in summer; k=19.4, r=0.995 for upwelling region in summer; k=17.3, r=0.991 for stations in autumn, respectively).

3.3 *Dual-isotopic composition of nitrate*

Depth profiles of nitrate δ^{15}N and δ^{18}O were generally similar between summer and autumn (Fig. 7a). The δ^{15}N presented a relatively high value of 6.0‰±0.1‰ at 500 m that was the water depth of the core of the NPIW in the SCS (You et al., 2005). Downward, the values of δ^{15}N decreased slowly and were stable below 1 500 m at 5.5‰; upward, δ^{15}N decreased more sharply to their minimum at 100 m water depth with the lowest values of 4.0‰ and 4.6‰ for summer and autumn, respectively; and the values between 100 m and 300 m was slightly lower in summer than that in autumn (p=0.006). Above 100 m, δ^{15}N increased severely to the maximum value of 12.0‰ for both seasons, however the overall values were significantly higher in autumn than those in summer (p=0.006; average values were 5.2‰±0.7‰, 6.8‰±2.5‰, and 7.9‰±2.2‰ for upwelling region, offshore stations in summer, and stations in autumn, respectively). The distribution trend of δ^{18}O below 500 m coincided with that of δ^{15}N and the value was 2.3‰±0.2‰ below 1 500 m. The values of δ^{15}N and δ^{18}O below 1 500 m in coastal waters of the EHI in summer and autumn were consistent with those in the world deep oceans (Sigman et al., 2009; Lehmann et al., 2018). However, δ^{18}O was relatively constant from 500 m to 100 m, which did not show a decreased trend and

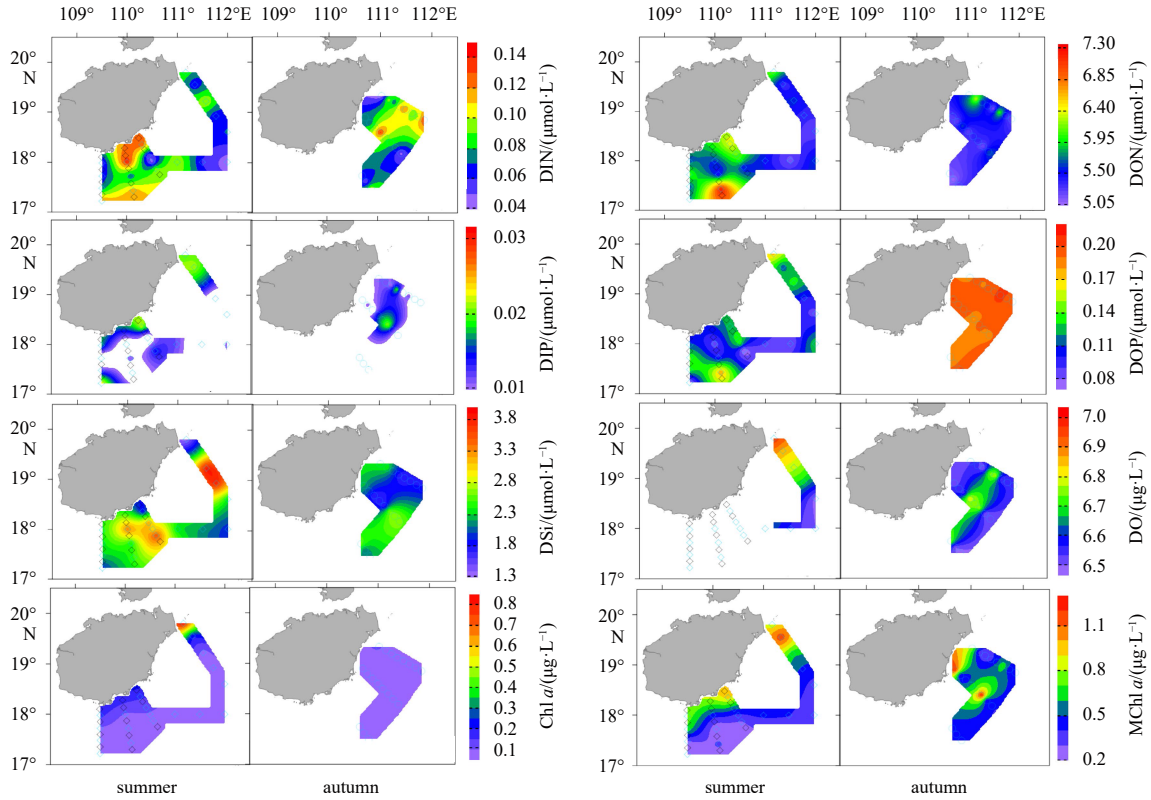

Fig. 4. Surface distribution of nutrients, Chl *a*, and DO concentrations in coastal waters of the eastern Hainan Island in summer and autumn. Concentration is below the detection limit in the blank area of DIP. We did not get the data of DO in the southern three sections in summer. MChl *a*: Chl *a* concentration at the depth of the Chl *a* maximum layer.

there were no obviously minimum values at 100 m water depth as the $\delta^{15}N$ did. Above 100 m, similar to $\delta^{15}N$, the values of $\delta^{18}O$ increased sharply, but the increased extent was bigger than that of $\delta^{15}N$; and also, the values of $\delta^{18}O$ in upwelling region were significantly lower than those in the summer offshore stations and stations in autumn (p<0.02; the average values were 3.7‰±1.4‰, 6.5‰±4.0‰, and 6.3‰±2.2‰ for upwelling region, summer offshore stations, and stations in autumn, respectively).

4 Discussion

4.1 *The vertical supply of nutrients caused by upwelling*

To comprehensively assess the importance of nutrients supplied by the coastal upwelling to the upper ocean for supporting the growth of plankton and primary production in coastal ecosystem of the EHI, we estimated ranges of the upwelled nutrient amounts from the aspects of nutrient dynamics and physical transport (Lips et al., 2009; Bombar et al., 2010; Su et al., 2011b).

4.1.1 *Estimation from the nutrient dynamics*

The amounts of nutrients supplied by upwelling could be overall estimated from the difference of the nutrient loads with and without the upwelling (Lips et al., 2009). The isopleths of hydrological and biogeochemical parameters along sections in September (just after the peak period of the upwelling; Figs S1 and S2), compared with those in July, were overall parallel to the water depth (Figs 2b and 5a). There were no significant differences in these parameters above 125 m (the upwelling influencing depth in summer) between offshore and nearshore stations (except for a weak difference in ammonium in Section A2 (p=0.047); Table S1), which strongly suggested that when there was no influence of the upwelling, the hydrological and biogeochemical conditions in the nearshore region in coastal waters of the EHI were similar to those in the offshore stations. Thus, we used the hydrological and biogeochemical parameters of offshore stations above 125 m in summer as the background parameters for nearshore stations, and the differences of these parameters between offshore (background) and nearshore stations in summer should be attributed to the effect of the upwelling. However, because the water depth became shallow toward the shore and the shape of water column along sections was irregular (Figs 2b and 5a), it was difficult to get the background conditions of those irregular sections from the offshore background stations. So, we took water depth of the shallowest station (S35, 50 m). We sampled in the upwelling region in summer to assess the nutrients supplied by upwelling to the upper ocean. This water depth is deeper than the MLD and shallower than the euphotic zone in the study area (Zhou, 2020); therefore, the upwelled nutrients within this water depth would be significant for nearby coastal ecosystem. Besides upwelling, the nearshore area could be affected by the river discharge, especially in the wet season. The Wanquan River is the largest river in the EHI, and reportedly, the low salinity (S<33) and high nutrient (e.g., DIN>1 μmol/L, DIP>0.1 μmol/L, and DSi>5 μmol/L, respectively) diluted water was limited within ~20 km off the estuary during July and September, and even within ~10 km for the smaller Wenchang River and Wenjiao River (Li et al., 2014). Indicated from our observation in September, the Wanquan River diluted water could not affect the coastal area we investigated (Figs 2a and 4). This finding corresponds with the study in similar region by Su et al.

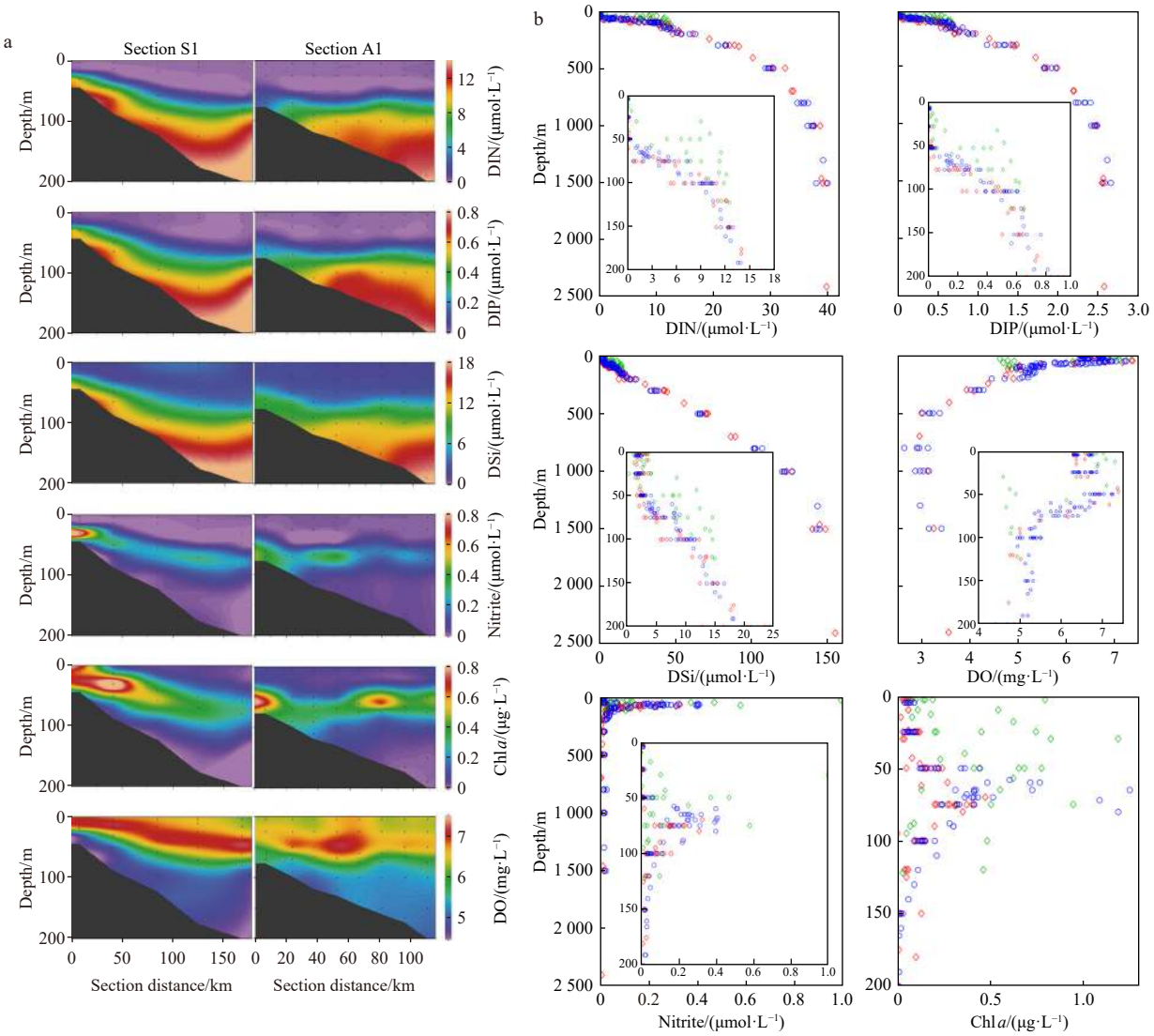

Fig. 5. The sectional distribution of biogeochemical parameters in the upper 200 m in Sections S1 in summer and A1 in autumn (a); depth profiles of biogeochemical parameters (b). The shapes and colors distinguished the samples as same as those in Fig. 3b. The inside figures were the same as their outside figures only with the water depth above 200 m to show the details.

(2011b) which reported that freshwaters from Wanquan River, Wenchang River, and Wenjiao River were confined to the coastal area with less than 20–30 m deep and estuarine water did not have a significant impact on upwelling strength on shelf of the EHI. Furthermore, considering that the average discharge and precipitation in the Wanquan River estuary are usually higher in September than in July (Li et al., 2013) and there is no river larger than the Wanquan River in the nearshore area of the three southern sections (i.e., S2 to S4), the coastal area of the investigation in July was unlikely to be affected by the river discharge either. The shallow water tongue (<25 m) from the southwest toward the northeast with slightly lower salinity (around 33.6–33.8) and higher DSi (around 2.4–3.8 μmol/L) than the surrounding water observed in July extended quite far off the shore (>100 km), and its DIN (<0.1 μmol/L) and DIP (<0.02 μmol/L) were rather low (Figs 2a and 4), which probably did not result from the river discharge in the EHI. Indicated from the images of SSS and SSV, the water tongue was probably originated from other riverine input in the western and northwestern SCS, such as the Beibu Gulf (Figs S1b and S2a). Though decomposition of organic carbon from these areas might provide nutrients (Huang et al., 2017), the low DIN and DIP in the water tongue implied that the consumption might be more pronounced and the contribution from these long-range transports in the study area should be limited.

The water depth weighted inorganic nutrient and Chl *a* concentrations above 50 m of upwelling stations were significantly higher than those of the background stations and the stations in autumn (Table 1). The difference of DSi between the upwelling and background stations was rather small compared with that of DIN and DIP, which might be due to the dominant fast-growing diatoms in the coastal upwelling regions during summer (Wu et al., 2014; Zhang et al., 2015) consumed DSi rapidly and the rate of the remineralization of Si-rich sinking particles was slow (Han et al., 2012). The bigger standard deviation (SD) of the inorganic nutrients and Chl *a* in the upwelling area was caused by the obvious onshore gradients (Fig. 5a). The relatively constant concentrations of DON and DOP among upwelling, the background stations, and the stations in autumn implied the biologically recalcitrant nature of dissolved organic matter (Knapp et al., 2005). By subtracting the background values from the nutrient concentra-

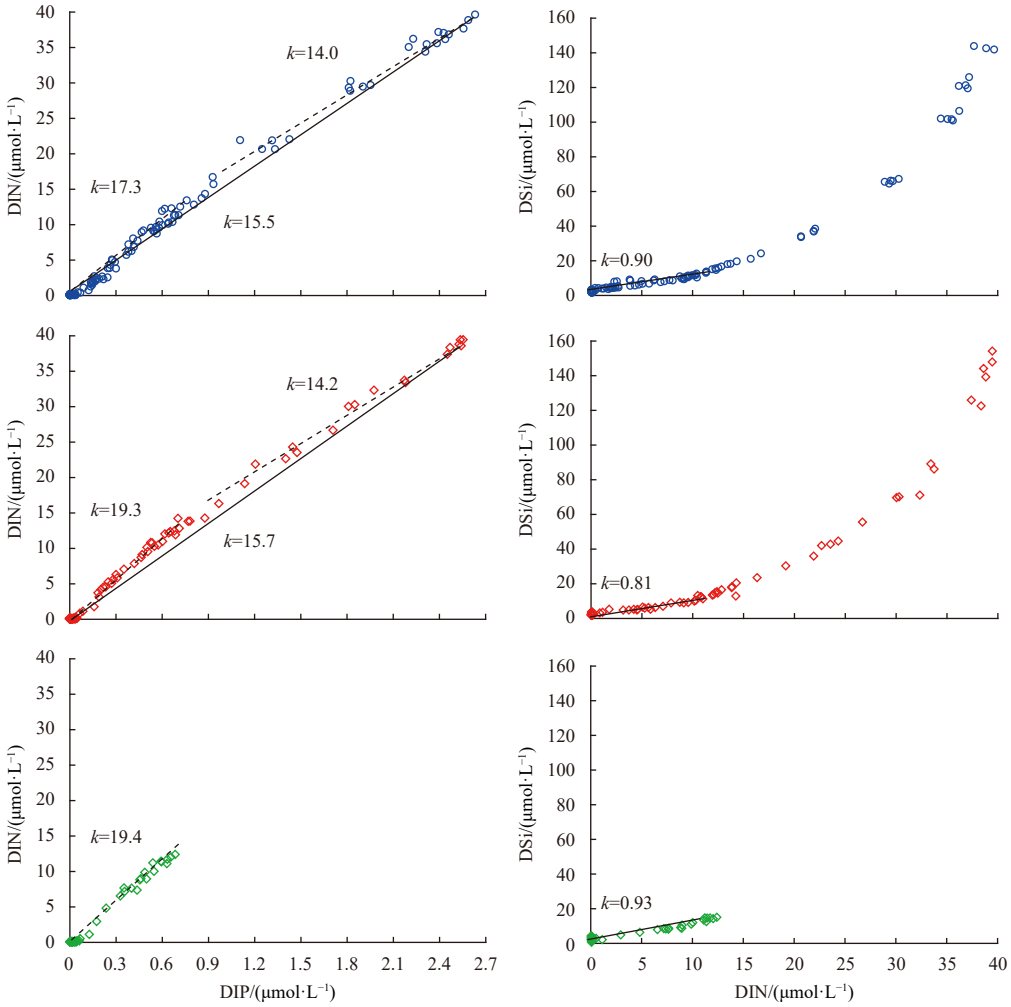

Fig. 6. Relationships between DIN and DIP as well as DSi and DIN. The shapes and colors distinguished the samples as same as those in Fig. 3b. The solid line was the regression curve for the whole water depth samples, and the dotted line was the regression curve for samples above and below the center of the North Pacific Tropical Water (~150 m). The slope was marked as the *k*.

tions of upwelling stations, the increased nutrient concentrations caused by the seasonal upwelling in coastal area of the EHI were (75.1±82.6) mmol/m², (4.47±4.63) mmol/m², and (66.0±67.1) mmol/m² for DIN, DIP, and DSi, respectively, which supported the additional growth of plankton for (14.7±8.95) mg/m² of Chl *a* in the upper 50 m. The DIN/DIP and DSi/DIN of the average increased nutrient concentrations caused by the upwelling were 16.8 and 0.9. Indicated from the SST, SSS, and SSV in 2015 (Figs S1 and S2a), the upwelling in coastal waters of the EHI was strongest during May to July, and the upwelling took approximate one month (April) to get its peak status (similar to the reports in Su and Pohlmann (2009) and Su et al. (2011b)). We took the increased nutrient concentrations represented the biogeochemical conditions during the peak period of the upwelling, then the fluxes of nutrients supplied by the coastal upwelling were (2.5±2.7) mmol/(m²·d), (0.15±0.15) mmol/(m²·d), and (2.2±2.2) mmol/(m²·d) for DIN, DIP, and DSi, respectively. Considering of the higher Chl *a* in nearshore stations than the background value and the nutrient consumption by planktons, the increased nutrient concentrations caused by the upwelling might be higher, especially when the upwelling just achieved its peak status, so the nutrient fluxes estimated by this way should be the lower limit.

4.1.2 *Estimation from the physical transport*

The vertical velocity of the upwelling at base of the mixed layer could be roughly estimated using the method suggested in Su et al. (2011b): the thickness of the mixed layer in the stations closest to the shore of each section was averaged 4 m and that in the outermost offshore stations of each section was averaged 29 m, then the mixed layer was uplifted 25 m by the coastal upwelling in April. Then, the overall vertical velocity of the upwelling at base of the mixed layer was simply estimated to be 0.83 m/d (25 m divided by 30 d, ca. 1×10^{-5} m/s). The upwelling in the ocean typically has the upward speed of 10^{-6} m/s to 10^{-4} m/s (Hu and Wang, 2016). The speed would exceed 4×10^{-4} m/s in the ocean near Peru where has one of the strongest upwelling system in the world (Albert et al., 2010; Wang et al., 2013). While for coastal waters of the northwestern SCS, the upward speed of upwelling was relatively lower, such as ranged from 1.6×10^{-5} m/s to 2.5×10^{-5} m/s in the 40 m to 100 m water depth of the southeastern Vietnamese coast (Bombar et al., 2010), and 0.7×10^{-5} m/s to 4.5×10^{-5} m/s within the tens of meters water depth of the coastal water of EHI (Deng et al., 1995; Guo et al., 1998; Han et al., 1990; Jing et al., 2009; Su et al., 2011b). Our result, though relatively lower, was within the reported results. The outermost stations of the four sections that affected by the upwelling were averaged

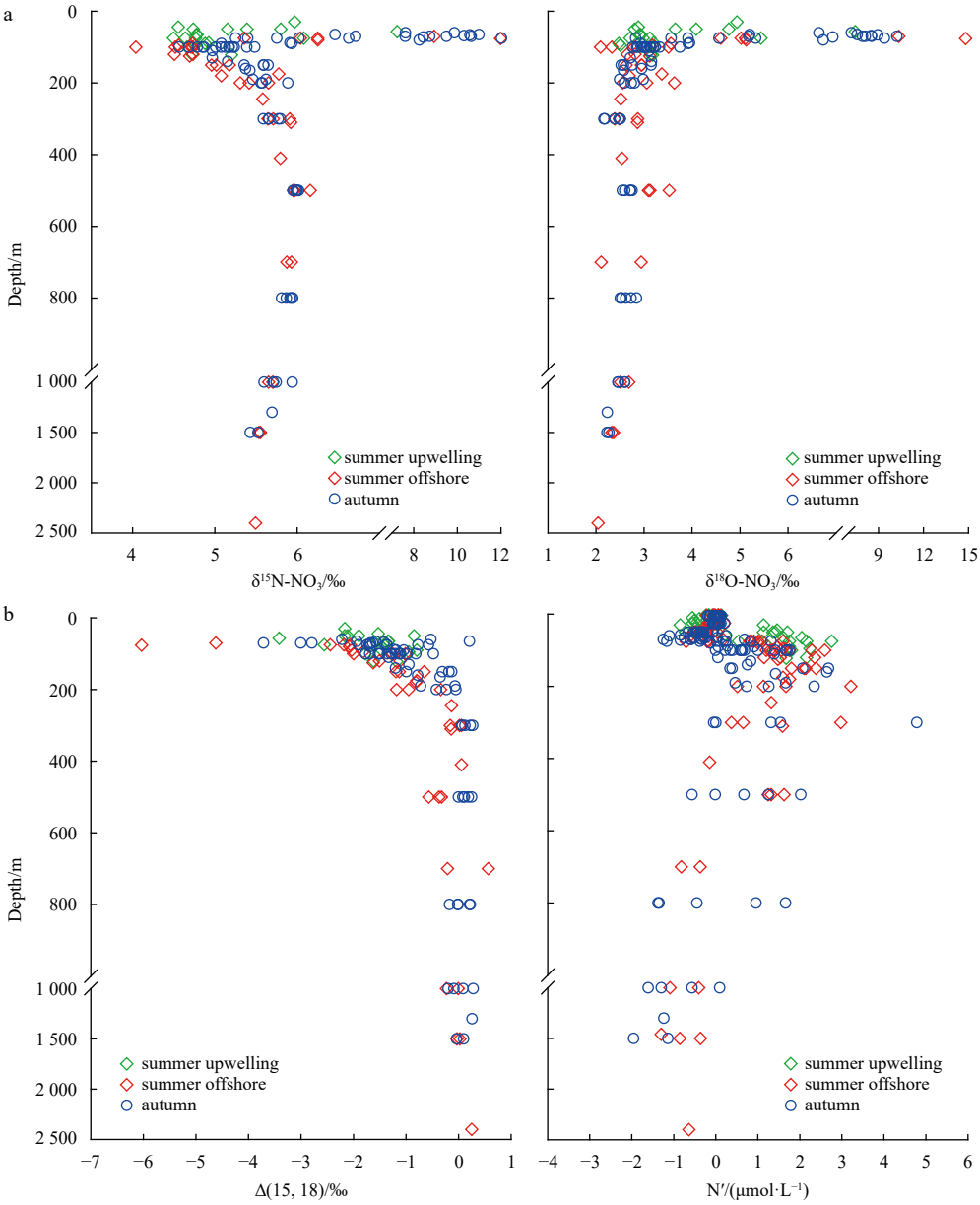

Fig. 7. Depth profiles for dual-isotopic composition of nitrate (a), Δ(15, 18) and nitrate concentration anomaly (N′) (b).

Table 1. Water depth weighted nutrient and Chl *a* concentrations above 50 m of the upwelling region and its background values, and of stations in autumn in coastal area of the eastern Hainan Island

		DIN/(μmol·L^{-1})	DIP/(μmol·L^{-1})	DSi/(μmol·L^{-1})	Chl *a*/(μg·L^{-1})	DON/(μmol·L^{-1})	DOP/(μmol·L^{-1})
Upwelling	average	1.59	0.10	3.88	0.39	5.69	0.13
	SD	1.65	0.09	1.23	0.18	0.28	0.02
Background	average	0.08	0.01	2.56	0.09	5.67	0.11
	SD	0.02	0.01	0.54	0.03	0.25	0.02
Autumn	average	0.16	0.01	2.35	0.11	5.62	0.19
	SD	0.12	0.01	0.33	0.04	0.54	0.01

about 60 km away from the shore and the length of the coastline in our study area was about 270 km, then the water flux entered the mixed layer driven by upwelling was 6.75×10^9 m^3/d (~0.08×10^6 m^3/s), which was slightly higher than that estimated by Su et al. (2011b) in summer 2007 and 2008. A decade (2000–2009) average total water flux uplifted by the upwelling in coastal area of the EHI estimated by Wang et al. (2013) was 0.21×10^6 m^3/s and based on our result, only ~37% of it entered the mixed layer. According to this result, the upwelling would uplift ~6.1×10^{11} m^3 water entered the mixed layer from below during its peak period (May to July), which was approximate 10 times bigger than the sum of the annual total riverine discharge in the Hainan Island into the SCS (ca. 3.1×10^{10} m^3, Zhang et al., 2013) and the annual rainfall in the study area (~3.2×10^{10} m^3, based on the annual rainfall of no more

than 2 000 mm and the study area of 60×270 km^2; Herbeck et al., 2020; Li et al., 2013, 2014; Liu et al., 2011; Zhang et al., 2006).

The nutrients supplied by upwelling could also be evaluated from the aspect of the upward physical transport (Bombar et al., 2010). $F_{upwelling}=v\times C_{nutrient}$, where v was the vertical velocity of the upwelling and $C_{nutrient}$ was the nutrient concentrations. We took 0.83 m/d (ca. 1×10^{-5} m/s) as the v in our calculation and the fluxes of nutrients supplied by the upwelling to the upper 50 m would be (4.18±3.24) mmol/(m^2·d), (0.23±0.16) mmol/(m^2·d), (5.59±2.67) mmol/(m^2·d), (4.58±0.60) mmol/(m^2·d), and (0.13±0.05) mmol/(m^2·d) for DIN, DIP, DSi, DON, and DOP, respectively. The fluxes of DIN and DIP calculated by this way were slightly higher than those entered the mixed layer estimated by Luo et al. (2018). The upwelled DIN/DIP and DSi/DIN (18 and 1.3) were slightly higher than those estimated from the nutrient dynamics, but also did not distinguish from the Redfield ratios. Furthermore, the vertical inorganic nutrient fluxes of background area (the offshore stations) could be estimated by considering the turbulent diffusion, which was calculated by combining the turbulent diffusion and vertical gradient of the nutrient concentration (Li et al., 2021) using the following: $F_{diffusion}=-Kz\times(\partial C_{nutrient}/\partial z)$, where Kz was the turbulent diffusion coefficient and the negative sign represented that direction of the diffusion was opposite to the concentration gradient direction; $\partial C_{nutrient}/\partial z$ was the gradient of nutrient concentrations, which was determined from differences of nutrient concentration and water depth. Kz was reported to be 1×10^{-4} m^2/s in the 30 m to 60 m water depth of the Vietnamese coast (Bombar et al., 2010) and in coastal waters of the EHI (Guo et al., 1998). Thus, the vertical nutrient fluxes of background area were (1.05±0.75) mmol/(m^2·d), (0.05±0.03) mmol/(m^2·d), and (0.68±0.43) mmol/(m^2·d) for DIN, DIP, and DSi, respectively. The inorganic nutrient fluxes supplied by the upwelling were several times higher than those by turbulent diffusion in the background area. It should be noted that the nutrient fluxes supplied by turbulent diffusion in the upwelling area, ((2.26±0.86) mmol/(m^2·d), (0.10±0.04) mmol/(m^2·d), and (2.25±0.62) mmol/(m^2·d) for DIN, DIP, and DSi, respectively) were also obviously higher than those in the background area. Considering that there were processes of nutrient addition and consumption (e.g., mineralization and assimilation) both in areas of upwelling and background, the high nutrient fluxes supplied by turbulent diffusion in the upwelling area should be attributed to the nearshore upwelling enhancing the nutrient concentration gradient of the upper ocean. Upwelling not only brought the nutrient-replete water to the upper ocean directly, but also further promoted the vertical nutrient fluxes of turbulent diffusion by enhancing the nutrient concentration gradient. Then, the total vertical nutrient fluxes in the upwelling area were around 6- to 12- fold those in the background area, which reflects the significance of upwellings to nearby coastal ecosystems.

Based on different approaches, the average nutrients entered the upper 50 m water depth in the coastal EHI arisen from the upwelling were estimated at the ranges of 2.5 mmol/(m^2·d) to 5.4 mmol/(m^2·d), 0.15 mmol/(m^2·d) to 0.28 mmol/(m^2·d), and 2.2 mmol/(m^2·d) to 7.2 mmol/(m^2·d) for DIN, DIP, and DSi, respectively. The upwelling nutrient fluxes were at least two orders of magnitude higher than the annual atmospheric nutrients input in the SCS (Wu et al., 2018; Chen et al., 2001). The average upwelled nutrient amounts during its peak period (May to July) were 5.8×10^9 mol for DIN, 3.1×10^8 mol for DIP, 6.8×10^9 mol for DSi, 6.7×10^9 mol for DON, and 1.8×10^8 mol for DOP. The inorganic nutrients were about 10 times higher than the annual nutrient fluxes transported from land to the coastal EHI estimated by Su et al. (2011a); and DIN and DSi were 10 times and 4 times, DIP, DON, and DOP were about 25 times higher than those of the total annual discharges from the Wenchang River estuary, Wenjiao River estuary, Wanquan River estuary, and Xiaohai Lagoon and Laoye Lagoon to the coastal EHI (Li et al., 2013, 2014; Liu et al., 2011). As nitrogen was the primary limited factor in upper ocean of the study area (the obviously low N/P and high Si/N above the DCM compared with those below), based on the Redfield ratio, the upwelled DIN could support 16.6 mmol/(m^2·d) to 35.8 mmol/(m^2·d) of carbon fixation. The primary production around our study area ranged from 26.4 mmol/(m^2·d) to 58.4 mmol/(m^2·d) (in terms of C) (Ning et al., 2004; Song et al., 2012; Zhang et al., 2015), which implied that, averagely, the carbon fixation supported by the upwelling in summer 2015 was about 62% of the primary production in the study area.

4.2 *Nitrogen cycling constrained by nitrate $\delta^{15}N$ and $\delta^{18}O$*

The nitrogen fixation, remineralization, nitrification, and assimilation are usually the most important nitrogen cycling processes in oxygen-rich water. The nitrate concentration and $\delta^{15}N$ synchronized decreased upward between 500 m and 100 m of the coastal water of EHI (Figs 5b and 7a). This similar trend was widely observed in the tropical and subtropical open oceans and was mainly attributed to the nitrogen fixation and its following remineralization and nitrification bringing ^{15}N depleted nitrogen sources to the upper ocean (Bourbonnais et al., 2009; Casciotti et al., 2008; Lehmann et al., 2018). While for the marginal seas, input from atmospheric deposition might be another important source of light nitrogen (Liu et al., 2017; Umezawa et al., 2014). For the SCS, the reported annual reactive nitrogen input from atmospheric deposition (around 9–50 mmol/(m^2·a); Kim et al., 2014; Yang et al., 2014) was comparable with the measured rate of nitrogen fixation (around 17–50 mmol/(m^2·a); Bombar et al., 2010; Chen et al., 2014; Voss et al., 2006; Zhang et al., 2015). Nitrogen fixation induces the $\delta^{15}N$ value of (–1‰±1‰) (Hoering and Ford, 1960; Minagawa and Wada, 1986) and atmospheric deposition led to slightly lower $\delta^{15}N$ values in the SCS (averagely, –2.7‰ for nitrate and –1.7‰ for ammonium; Jia and Chen, 2010; Yang et al., 2014). Both of them were significantly lower than the average $\delta^{15}N$ in the world oceans (4.7‰, Altabet, 2006). However, the $\delta^{18}O$ in atmospheric deposition ranged from 59‰ to 79‰ (Yang et al., 2014), which was extremely high compared with the $\delta^{18}O$ in the world oceans, whereas the $\delta^{18}O$ introduced by nitrification was similar to or slightly higher (around 1.1‰–1.3‰) than its ambient water (Buchwald et al., 2012; Casciotti et al., 2008; Marconi et al., 2019; Sigman et al., 2009). Though the $\delta^{18}O$ was as high as nearly 15‰ above 100 m water depth, the concomitant of high $\delta^{15}N$ implied that algal nitrate assimilation was the reason causing the high $\delta^{18}O$ (see below). Combined with the low DIN concentration and DIN/DIP within the mixed layer (Figs 5b and 6), the reactive nitrogen from atmospheric deposition should be assimilated rapidly. Nitrogen fixation (and atmospheric deposition) and the following degradation of N-rich organic matter would result in higher DIN/DIP and lower DSi/DIN above the NPTW (Wong et al., 2007), thus, the higher slope of DIN to DIP and lower of DSi to DIN above the NPTW in summer than that in autumn (Fig. 6) probably resulted from the stronger nitrogen fixation (Chen et al., 2008) and atmospheric deposition in summer than autumn in the SCS (the high slope of DSi to DIN in upwelling region in summer was resulted from the southwestern high DSi and low salinity water tongue). Together with the higher biological activities (indicated from the Chl *a* and nitrite, Fig. 5b and Section 3.2.1) in the upper ocean in autumn than back-

ground stations in summer (Shen et al., 2008; Cai et al., 2015; Li et al., 2018) resulted in the higher $\delta^{15}N$ values in autumn than summer above 300 m (Fig. 7a). The $\delta^{15}N$ and $\delta^{18}O$ of nearshore stations in summer were significantly lower than those of offshore stations and stations in autumn, which probably attributed to that more nitrate was supplied to the nearshore stations by upwelling and the nitrate from below had relatively lower $\delta^{15}N$ and $\delta^{18}O$ (Figs 5b and 7a). The obvious spatial and temporal differences of nitrate isotope composition above 300 m water depth (top of the NPIW) implied the nitrogen cycling was sensitive to the environmental conditions in the upper ocean.

Nitrate isotope anomaly, $\Delta(15, 18)=(\delta^{15}N_{nitrate}-\delta^{15}N_m)-{}^{15}\varepsilon/{}^{18}\varepsilon\times(\delta^{18}O_{nitrate}-\delta^{18}O_m)$ (Sigman et al., 2005) was widely used to analyze the processes that drove the relationship of $\delta^{15}N_{nitrate}$ and $\delta^{18}O_{nitrate}$ deviated from the 1:1 pattern caused by nitrate consumption (e.g., assimilation and denitrification; Granger et al., 2004, 2008; Sigman et al., 2005), where $\delta^{15}N_m$ and $\delta^{18}O_m$ were the nitrate isotope composition sourced from the deep ocean. Because of the seasonal stability for nitrate isotope composition in deep ocean near the EHI (Fig. 7a), we took 5.5‰ and 2.3‰ as the $\delta^{15}N_m$ and $\delta^{18}O_m$ in our calculations. Meanwhile, the nitrate anomaly relative to DIP, $N'=[DIN]-k\times[DIP]$, could reflect the processes of nitrogen addition and removal in the ocean (Deutsch et al., 2001; Gruber and Sarmiento, 1997), where k was the slope of the linear regression of DIN and DIP in the study area (Fig. 6). The $\Delta(15, 18)$ was relatively constant below 300 m water depth for both seasons with average value of (0.0‰±0.2‰) (Fig. 7b). Above 300 m, $\Delta(15, 18)$ decreased upward and the values in summer were significantly lower than those in autumn (p=0.018; the minimum values for summer and autumn were –6.0‰ and –3.7‰, respectively); meanwhile, the N' presented the maximum values around the 300 m water depth (Fig. 7b) and the values in summer were significantly higher than those in autumn (p=0.000). The average values of $\Delta(15, 18)$ and N' above 300 m in summer and autumn were –1.5‰±1.1‰, (1.43±0.69) μmol/L and –1.1‰±0.8‰, (0.66±1.06) μmol/L, respectively. The higher N' in summer indicated the higher new nitrogen inputs from nitrogen fixation and atmospheric deposition as well as the following nitrate regeneration affected the nutrient compositions deep to 300 m. The nitrate originated from the nitrogen fixation and atmospheric deposition would decrease the values of $\Delta(15, 18)$ by adding more negative ^{15}N relative to ^{18}O, which probably was the main reason for the lower $\Delta(15, 18)$ in summer than autumn. For coastal waters of the EHI, the decreased $\Delta(15, 18)$ in the upper ocean might also be caused by the cycles of incomplete nitrate assimilation and regeneration (Casciotti et al., 2008). The relationships between nitrate $\delta^{18}O$ and $\delta^{15}N$ for samples above the NPTW (center at around 100 m to 150 m) presented linearly both in summer and autumn (Fig. 8a). The salinity decreased upward and downward from the NPTW (Fig. 3a) together with the differences of slopes for regressions of DIN to DIP and DSi to DIN above and below the NPTW (Fig. 6) implied the processes of remineralization and mixing between the waters above and below the NPTW were different, and the algal nitrate assimilation regulated the nitrate isotope composition just above the NPTW. The $\delta^{18}O$:$\delta^{15}N$ above the NPTW in autumn was nearly the same as that expected from nitrate consumption of 1:1, which indicated the assimilation was the dominated nitrogen cycling process above the NPTW in autumn (Fig. 8a). While in the summer, the higher $\delta^{18}O$:$\delta^{15}N$ above the NPTW (1.6 to 1.7) implied the nitrification was more important compared with the autumn (Granger and Wankel, 2016; Liu et al., 2017; Umezawa et al., 2014; Wankel et al., 2007).

The open and closed systems of Rayleigh model (Eqs (1) and (2)) were applied to get the isotopic effect of algal nitrate assimilation. For the upwelling stations in summer, nitrate was provided by the coastal upwelling continuously, so we attempted to use the open Rayleigh model to get the isotopic fractionation factor. Then the f could be computed as the nitrate measured in the upwelling stations divided by the initial upwelled nitrate. Because of the depth of the upwelling extended to at least 125 m (Figs 3b and 5b), which at the center of the NPTW, we took the concentrations of nitrate at the NPTW as the initial nitrate concentration for upwelling stations in summer. For the background stations in summer and all stations in autumn, we applied the closed system model. As the initial nitrate concentration is a constant value, the Eq. (2) could be written as $\delta^{15}N\ (\delta^{18}O)=\delta^{15}N\ (\delta^{18}O)_{f=1}+{}^{15}\varepsilon({}^{18}\varepsilon)\times\ln[NO_3^-]_i-{}^{15}\varepsilon\ ({}^{18}\varepsilon)\times\ln[NO_3^-]_m$, where $[NO_3^-]_i$ and $[NO_3^-]_m$ were the concentrations of initial nitrate and measured nitrate above the NPTW. Then the slope of the linear regression for $\delta^{15}N$ ($\delta^{18}O$) and $\ln[NO_3^-]_m$ could be regarded as the ${}^{15}\varepsilon$ (${}^{18}\varepsilon$) in the closed system model. The ${}^{15}\varepsilon$ and ${}^{18}\varepsilon$ were estimated to be 2.2‰ and 3.9‰, 3.0‰ and 4.9‰, and 3.1‰ and 3.4‰ for upwelling, background stations in summer, and all stations in autumn, respectively (Fig. 8b). The isotopic fractionation factors of nitrate nitrogen and oxygen were obviously smaller in upwelling stations than those in background stations in summer, which was probably arisen from the difference of plankton species between the two areas and the isotopic fractionation factors for nitrate assimilation were variable between plankton species (Granger et al., 2004). The diatoms were reported to be favored with the nutrient abundance environment and were the dominant species in coastal upwelling regions (Umezawa et al., 2014; Wu et al., 2014; Zhang et al., 2015) and some species were with relatively small isotopic fractionation factor when proceeding the nitrate assimilation (e.g., ~2.7‰ for *Chaetoceros* spp.; Needoba et al., 2003). Reportedly, diatom accounted for about half of phytoplankton biomass at the upwelling area of the coastal water of EHI in summer 2015 and its abundance was decreased to ~10% at the offshore area (Liu et al., 2020a). Additionally, the ${}^{15}\varepsilon$ was lower than ${}^{18}\varepsilon$ in all three conditions, which was probably due to the nitrification of fixed nitrogen from nitrogen fixation and atmospheric deposition introduced nitrate with lower ^{15}N relative to ^{18}O, and increased the nitrate concentration simultaneously. Furthermore, compared with the autumn, the difference between ${}^{15}\varepsilon$ and ${}^{18}\varepsilon$ were significantly larger in summer (averagely 1.8‰ for summer and 0.3‰ for autumn), which was another evidence for the stronger nitrogen fixation and atmospheric deposition and the following nitrate regeneration in summer than in autumn.

5 Conclusions

The upwelling in the coastal EHI in summer 2015 extended to the water depth of at least 125 m and distance of 50 km to 85 km away from the shore. The values of nutrients and Chl *a* in upwelling influencing area were significantly higher than non-upwelling area. Estimated from aspects of nutrient dynamics and physical transport, the nutrients entered the upper 50 m water depth arisen from the upwelling averagely ranged from 2.5 mmol/(m²·d) to 5.4 mmol/(m²·d), 0.15 mmol/(m²·d) to 0.28 mmol/(m²·d), and 2.2 mmol/(m²·d) to 7.2 mmol/(m²·d) for DIN, DIP, and DSi, respectively, which supported the additional growth of plankton for (14.7±8.95) mg/m² of Chl *a*, and the DIN could support, maximally, 62% of the primary production in the study area. The vertical nutrient fluxes in the upwelling area were around 6- to 12-fold those in the background area.

The distributions of nitrate $\delta^{15}N$ and $\delta^{18}O$ below 300 m water

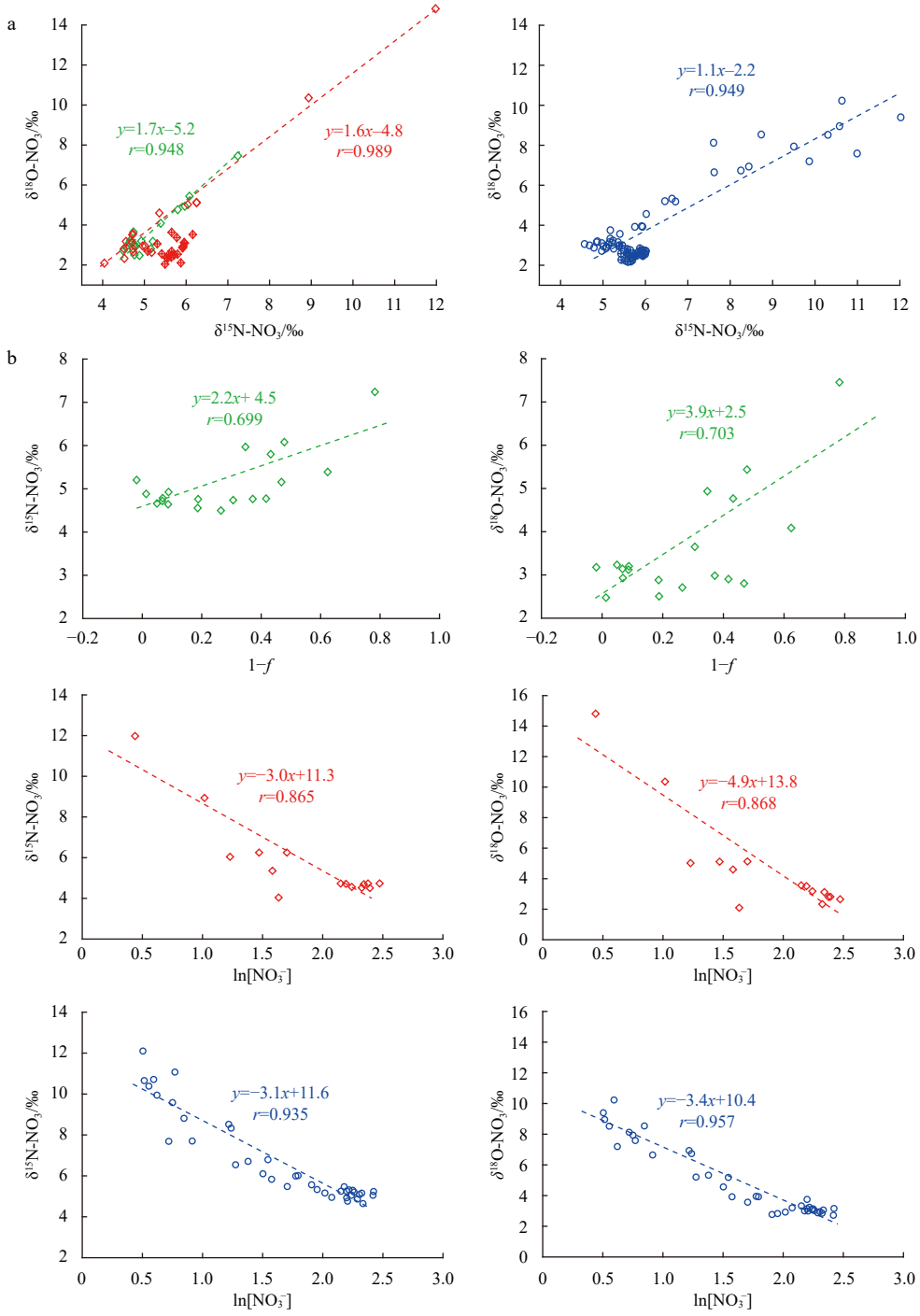

Fig. 8. The relationships between the nitrate $\delta^{18}O$ and $\delta^{15}N$ (a); and between $\delta^{15}N$, $\delta^{18}O$, and 1-*f*; $\delta^{15}N$, $\delta^{18}O$, and $\ln[NO_3^-]$ (b). The green and red rhombuses, and blue circles stood for the upwelling and background stations in summer, and all stations in autumn above the North Pacific Tropical Water (NPTW). The dotted lines and equations were the linear regressions for samples above the NPTW. The rhombuses and circles with cross inside in a were samples below the NPTW. The slopes in b were regarded as the isotope fractionation factor (ε). The *f* was the fraction of unassimilated nitrate in the water column.

depth (top of the NPIW) were stable among seasons in coastal area of the EHI, while above the NPIW, the nitrogen cycling processes were different between summer and autumn. The $^{15}\varepsilon$ and $^{18}\varepsilon$ of nitrate assimilation were estimated to be 2.2‰ and 3.9‰, 3.0‰ and 4.9‰, and 3.1‰ and 3.4‰ for upwelling stations, background stations in summer, and all stations in autumn, respectively. The larger difference between $^{15}\varepsilon$ and $^{18}\varepsilon$ in summer than that in autumn along with the higher DIN/DIP and $\delta^{18}O$:$\delta^{15}N$ above the NPTW; the lower $\delta^{15}N$ and $\Delta(15, 18)$, and higher N′ above the NPIW in summer strongly suggested the nitrogen fixation and atmospheric deposition, and the following remineralization and nitrification were stronger in summer. Nevertheless, the nitrate assimilation was stronger in autumn than background area in summer, which made the nitrate isotopes in the upper ocean higher in autumn, and the $\delta^{18}O$:$\delta^{15}N$ close to the ratio that was expected from nitrate assimilation.

Acknowledgements

We are grateful to Zhaomeng Xu and Yuwei Ma for their help with field studies. We greatly acknowledge the crew members of the R/V *Shiyan3* for their assistance, all the participants for their help and contribution during the investigation.

References

Albert A, Echevin V, Lévy M, et al. 2010. Impact of nearshore wind stress curl on coastal circulation and primary productivity in the Peru upwelling system. Journal of Geophysical Research: Oceans, 115(C12): C12033, doi: 10.1029/2010JC006569

Altabet M A. 2006. Isotopic tracers of the marine nitrogen cycle: present and past. In: Volkman J K, ed. Marine Organic Matter: Biomarkers, Isotopes and DNA. Berlin: Springer, 251–293

Bombar D, Dippner J W, Doan H N, et al. 2010. Sources of new nitrogen in the Vietnamese upwelling region of the South China Sea. Journal of Geophysical Research: Oceans, 115(C6): C06018

Bourbonnais A, Lehmann M F, Hamme R C, et al. 2013. Nitrate elimination and regeneration as evidenced by dissolved inorganic nitrogen isotopes in Saanich Inlet, a seasonally anoxic fjord. Marine Chemistry, 157: 194–207, doi: 10.1016/j.marchem.2013.09.006

Bourbonnais A, Lehmann M F, Waniek J J, et al. 2009. Nitrate isotope anomalies reflect N_2 fixation in the Azores Front region (subtropical NE Atlantic). Journal of Geophysical Research: Oceans, 114(C3): C03003

Buchwald C, Santoro A E, McIlvin M R, et al. 2012. Oxygen isotopic composition of nitrate and nitrite produced by nitrifying cocultures and natural marine assemblages. Limnology and Oceanography, 57(5): 1361–1375, doi: 10.4319/lo.2012.57.5.1361

Cai Pinghe, Zhao Daochen, Wang Lei, et al. 2015. Role of particle stock and phytoplankton community structure in regulating particulate organic carbon export in a large marginal sea. Journal of Geophysical Research: Oceans, 120(3): 2063–2095, doi: 10.1002/2014JC010432

Casciotti K L, Buchwald C, McIlvin M. 2013. Implications of nitrate and nitrite isotopic measurements for the mechanisms of nitrogen cycling in the Peru oxygen deficient zone. Deep-Sea Research Part I: Oceanographic Research Papers, 80: 78–93, doi: 10.1016/j.dsr.2013.05.017

Casciotti K L, Sigman D M, Hastings M G, et al. 2002. Measurement of the oxygen isotopic composition of nitrate in seawater and freshwater using the denitrifier method. Analytical Chemistry, 74(19): 4905–4912, doi: 10.1021/ac020113w

Casciotti K L, Trull T W, Glover D M, et al. 2008. Constraints on nitrogen cycling at the subtropical North Pacific Station ALOHA from isotopic measurements of nitrate and particulate nitrogen. Deep-Sea Research Part II: Topical Studies in Oceanography, 55(14–15): 1661–1672, doi: 10.1016/j.dsr2.2008.04.017

Chai Fei, Xue Huijie, Shi Maochong. 2001. Upwelling east of Hainan Island. In: Xue Huijie, Chai Fei, Xu Jianping, eds. Oceanography in China (13)—South China Sea Circulation Modeling and Observations. Beijing: China Ocean Press, 129–137

Chavez F P, Toggweiler J R. 1995. Physical estimates of global new production: the upwelling contribution. In: Summerhayes C P, Emeis K C, Angel M V, et al., eds. Upwelling in the Ocean: Modern Processes and Ancient Records. Chichester: Wiley, 313–320

Chen Yuh-ling Lee, Chen Houng-Yung, Lin Yen-Huei, et al. 2014. The relative contributions of unicellular and filamentous diazotrophs to N_2 fixation in the South China Sea and the upstream Kuroshio. Deep-Sea Research Part I: Oceanographic Research Papers, 85: 56–71, doi: 10.1016/j.dsr.2013.11.006

Chen Yuh-ling Lee, Chen Houng Yung, Tuo Sing-how, et al. 2008. Seasonal dynamics of new production from Trichodesmium N_2 fixation and nitrate uptake in the upstream Kuroshio and South China Sea basin. Limnology and Oceanography, 53(5): 1705–1721, doi: 10.4319/lo.2008.53.5.1705

Chen Fajin, Lao Qibin, Zhang Shuwen, et al. 2020. Nitrate sources and biogeochemical processes identified using nitrogen and oxygen isotopes on the eastern coast of Hainan Island. Continental Shelf Research, 207: 104209, doi: 10.1016/j.csr.2020.104209

Chen Chen-Tung Arthur, Wang Shu-Lun, Wang Bing-Jye, et al. 2001. Nutrient budgets for the South China Sea basin. Marine Chemistry, 75(4): 281–300, doi: 10.1016/S0304-4203(01)00041-X

Deng Song, Zhong Huanliang, Wang Mingwen, et al. 1995. On relation between upwelling off Qionghai and fishery. Journal of Oceanography in Taiwan Strait, 14(1): 51–56

Deutsch C, Gruber N, Key R M, et al. 2001. Denitrification and N_2 fixation in the Pacific Ocean. Global Biogeochemical Cycles, 15(2): 483–506, doi: 10.1029/2000GB001291

Granger J, Sigman D M, Lehmann M F, et al. 2008. Nitrogen and oxygen isotope fractionation during dissimilatory nitrate reduction by denitrifying bacteria. Limnology and Oceanography, 53(6): 2533–2545, doi: 10.4319/lo.2008.53.6.2533

Granger J, Sigman D M, Needoba J A, et al. 2004. Coupled nitrogen and oxygen isotope fractionation of nitrate during assimilation by cultures of marine phytoplankton. Limnology and Oceanography, 49(5): 1763–1773, doi: 10.4319/lo.2004.49.5.1763

Granger J, Wankel S D. 2016. Isotopic overprinting of nitrification on denitrification as a ubiquitous and unifying feature of environmental nitrogen cycling. Proceedings of the National Academy of Sciences of the United States of America, 113(42): E6391–E6400

Gruber N, Sarmiento J L. 1997. Global patterns of marine nitrogen fixation and denitrification. Global Biogeochemical Cycles, 11(2): 235–266, doi: 10.1029/97GB00077

Guan Bingxian, Chen Shangji. 1964. Ocean Current System in East China Sea and South China Sea (in Chinese). Qingdao: The Institute of Oceanology, Chinese Academy of Sciences, 1–85

Guo Fei, Shi Maochong, Xia Zongwan. 1998. Two-demension diagnose model to calculate upwelling on offshore of the east coast of Hainan Island. Haiyang Xuebao (in Chinese), 20(6): 109–116

Han Aiqin, Dai Minhan, Kao S J, et al. 2012. Nutrient dynamics and biological consumption in a large continental shelf system under the influence of both a river plume and coastal upwelling. Limnology and Oceanography, 57(2): 486–502, doi: 10.4319/lo.2012.57.2.0486

Han Wuying, Wang Mingbiao, Ma Kemei. 1990. On the lowest surface water temperature area of China sea in summer—The upwelling along the east coast of Hainan Island. Oceanologia et Limnologia Sinica, 21(3): 267–275

Herbeck L S, Krumme U, Andersen T J, et al. 2020. Decadal trends in mangrove and pond aquaculture cover on Hainan (China) since 1966: mangrove loss, fragmentation and associated biogeochemical changes. Estuarine, Coastal and Shelf Science, 233: 106531

Hoering T C, Ford H T. 1960. The isotope effect in the fixation of nitrogen by azotobacter. Journal of the American Chemical Society, 82(2): 376–378, doi: 10.1021/ja01487a031

Hu Jianyu, Wang Xiaohua. 2016. Progress on upwelling studies in the China seas. Reviews of Geophysics, 54(3): 653–673, doi: 10.1002/2015RG000505

Huang Ting-Hsuan, Chen Chen-Tung Arthur, Tseng Hsiao Chun, et al. 2017. Riverine carbon fluxes to the South China Sea. Journal of Geophysical Research: Biogeosciences, 122(5): 1239–1259, doi: 10.1002/2016JG003701

Jia Guodong, Chen Fajin. 2010. Monthly variations in nitrogen isotopes of ammonium and nitrate in wet deposition at Guangzhou, south China. Atmospheric Environment, 44(19): 2309–2315, doi: 10.1016/j.atmosenv.2010.03.041

Jing Zhiyou, Qi Yiquan, Du Yan. 2011. Upwelling in the continental shelf of northern South China Sea associated with 1997–1998 El Niño. Journal of Geophysical Research: Oceans, 116(C2): C02033

Jing Zhiyou, Qi Yiyuan, Hua Zulin, et al. 2009. Numerical study on the summer upwelling system in the northern continental shelf of the South China Sea. Continental Shelf Research, 29(2): 467–478, doi: 10.1016/j.csr.2008.11.008

Kara A B, Rochford P A, Hurlburt H E. 2000. An optimal definition for ocean mixed layer depth. Journal of Geophysical Research:

Oceans, 105(C7): 16803–16821, doi: 10.1029/2000JC900072
Kérouel R, Aminot A. 1997. Fluorometric determination of ammonia in sea and estuarine waters by direct segmented flow analysis. Marine Chemistry, 57(3–4): 265–275, doi: 10.1016/S0304-4203(97)00040-6
Kim T W, Lee K, Duce R, et al. 2014. Impact of atmospheric nitrogen deposition on phytoplankton productivity in the South China Sea. Geophysical Research Letters, 41(9): 3156–3162, doi: 10.1002/2014GL059665
Knapp A N, Sigman D M, Lipschultz F. 2005. N isotopic composition of dissolved organic nitrogen and nitrate at the Bermuda Atlantic Time-series study site. Global Biogeochemical Cycles, 19(1): GB1018
Lehmann N, Granger J, Kienast M, et al. 2018. Isotopic Evidence for the evolution of subsurface nitrate in the western equatorial Pacific. Journal of Geophysical Research: Oceans, 123(3): 1684–1707, doi: 10.1002/2017JC013527
Li Teng, Bai Yan, He Xianqiang, et al. 2018. The Relationship between POC export efficiency and primary production: opposite on the shelf and basin of the northern South China Sea. Sustainability, 10(10): 3634, doi: 10.3390/su10103634
Li Ruihuan, Liu Sumei, Li Yanwei, et al. 2014. Nutrient dynamics in tropical rivers, lagoons, and coastal ecosystems of eastern Hainan Island, South China Sea. Biogeosciences, 11(2): 481–506, doi: 10.5194/bg-11-481-2014
Li Ruihuan, Liu Sumei, Zhang Guiling, et al. 2013. Biogeochemistry of nutrients in an estuary affected by human activities: the Wanquan River estuary, eastern Hainan Island, China. Continental Shelf Research, 57: 18–31, doi: 10.1016/j.csr.2012.02.013
Li Ruihuan, Xu Jie, Cen Xianrong, et al. 2021. Nitrate fluxes induced by turbulent mixing in dipole eddies in an oligotrophic ocean. Limnology and Oceanography, 66(7): 2842–2854, doi: 10.1002/lno.11794
Lin Peigen, Cheng Peng, Gan Jianping, et al. 2016. Dynamics of wind-driven upwelling off the northeastern coast of Hainan Island. Journal of Geophysical Research: Oceans, 121(2): 1160–1173, doi: 10.1002/2015JC011000
Lips I, Lips U, Liblik T. 2009. Consequences of coastal upwelling events on physical and chemical patterns in the central Gulf of Finland (Baltic Sea). Continental Shelf Research, 29(15): 1836–1847, doi: 10.1016/j.csr.2009.06.010
Liu Sumei, Altabet M A, Zhao Liang, et al. 2017. Tracing nitrogen biogeochemistry during the beginning of a spring phytoplankton bloom in the Yellow Sea using coupled nitrate nitrogen and oxygen isotope ratios. Journal of Geophysical Research: Biogeosciences, 122(10): 2490–2508, doi: 10.1002/2016JG003752
Liu Sumin, Hong Bo, Wang Guifen, et al. 2020a. Physical structure and phytoplankton community off the eastern Hainan coast during summer 2015. Acta Oceanologica Sinica, 39(11): 103–114, doi: 10.1007/s13131-020-1668-z
Liu Sumei, Li Ruihuan, Zhang Guiling, et al. 2011. The impact of anthropogenic activities on nutrient dynamics in the tropical Wenchanghe and Wenjiaohe Estuary and Lagoon system in East Hainan, China. Marine Chemistry, 125(1–4): 49–68, doi: 10.1016/j.marchem.2011.02.003
Liu Sumei, Ning Xiaoyan, Dong Shuhang, et al. 2020b. Source versus recycling influences on the isotopic composition of nitrate and nitrite in the East China Sea. Journal of Geophysical Research: Oceans, 125(8): e2020JC016061
Liu Yi, Peng Zicheng, Shen Chuanchou, et al. 2013. Recent 121-year variability of western boundary upwelling in the northern South China Sea. Geophysical Research Letters, 40(12): 3180–3183, doi: 10.1002/grl.50381
Liu Kon-Kee, Su Mei-Jwen, Hsueh Chen-Ru, et al. 1996. The nitrogen isotopic composition of nitrate in the Kuroshio water northeast of Taiwan: evidence for nitrogen fixation as a source of isotopically light nitrate. Marine Chemistry, 54(3–4): 273–292, doi: 10.1016/0304-4203(96)00034-5
Loick N, Dippner J, Doan H N, et al. 2007. Pelagic nitrogen dynamics in the Vietnamese upwelling area according to stable nitrogen and carbon isotope data. Deep-Sea Research Part I: Oceanographic Research Papers, 54(4): 596–607, doi: 10.1016/j.dsr.2006.12.009
Luo Xin, Jiao J J, Liu Yi, et al. 2018. Evaluation of water residence time, submarine groundwater discharge, and maximum new production supported by groundwater borne nutrients in a coastal upwelling shelf system. Journal of Geophysical Research: Oceans, 123(1): 631–655, doi: 10.1002/2017JC013398
Marconi D, Weigand M A, Sigman D M. 2019. Nitrate isotopic gradients in the North Atlantic Ocean and the nitrogen isotopic composition of sinking organic matter. Deep-Sea Research Part I: Oceanographic Research Papers, 145: 109–124, doi: 10.1016/j.dsr.2019.01.010
Mariotti A, Germon J C, Hubert P, et al. 1981. Experimental determination of nitrogen kinetic isotope fractionation: some principles; illustration for the denitrification and nitrification processes. Plant and Soil, 62(3): 413–430, doi: 10.1007/BF02374138
McGregor H V, Dima M, Fischer H W, et al. 2007. Rapid 20th-century increase in coastal upwelling off Northwest Africa. Science, 315(5812): 637–639, doi: 10.1126/science.1134839
Minagawa M, Wada E. 1986. Nitrogen isotope ratios of red tide organisms in the East China Sea: a characterization of biological nitrogen fixation. Marine Chemistry, 19(3): 245–259, doi: 10.1016/0304-4203(86)90026-5
Needoba J A, Waser N A, Harrison P J, et al. 2003. Nitrogen isotope fractionation in 12 species of marine phytoplankton during growth on nitrate. Marine Ecology Progress Series, 255(24): 81–91
Ning Xiuren, Chai Fei, Xue Huijie, et al. 2004. Physical-biological oceanographic coupling influencing phytoplankton and primary production in the South China Sea. Journal of Geophysical Research: Oceans, 109(C10): C10005, doi: 10.1029/2004JC002365
Parsons T R, Maita Y, Lalli C M. 1984. A Manual of Chemical and Biological Methods for Seawater Analysis. Oxford: Pergamon Press, 173
Pauly D, Christensen V. 1995. Primary production required to sustain global fisheries. Nature, 374(6519): 255–257, doi: 10.1038/374255a0
Shen S H, Leptoukh G G, Acker J G, et al. 2008. Seasonal variations of chlorophyll *a* concentration in the northern South China Sea. IEEE Geoscience and Remote Sensing Letters, 5(2): 315–319, doi: 10.1109/LGRS.2008.915932
Sigman D M, Casciotti K L, Andreani M, et al. 2001. A bacterial method for the nitrogen isotopic analysis of nitrate in seawater and freshwater. Analytical Chemistry, 73(17): 4145–4153, doi: 10.1021/ac010088e
Sigman D M, DiFiore P J, Hain M P, et al. 2009. The dual isotopes of deep nitrate as a constraint on the cycle and budget of oceanic fixed nitrogen. Deep-Sea Research Part I: Oceanographic Research Papers, 56(9): 1419–1439, doi: 10.1016/j.dsr.2009.04.007
Sigman D M, Granger J, DiFiore P J, et al. 2005. Coupled nitrogen and oxygen isotope measurements of nitrate along the eastern North Pacific margin. Global Biogeochemical Cycle, 19(4): GB4022
Song Xingyu, Lai Zhigang, Ji Rubao, et al. 2012. Summertime primary production in northwest South China Sea: Interaction of coastal eddy, upwelling and biological processes. Continental Shelf Research, 48: 110–121, doi: 10.1016/j.csr.2012.07.016
Su Ni, Du Jinzhou, Ji Tao, et al. 2011a. ^{226}Ra and ^{228}Ra tracer study on nutrient transport in east coastal waters of Hainan Island, China. Water Science and Engineering, 4(2): 157–169
Su Jian, Pohlmann T. 2009. Wind and topography influence on an upwelling system at the eastern Hainan coast. Journal of Geophysical Research: Oceans, 114(C6): C06017
Su Jian, Wang Jun, Pohlmann T, et al. 2011b. The influence of meteorological variation on the upwelling system off eastern Hainan during summer 2007–2008. Ocean Dynamics, 61(6): 717–730, doi: 10.1007/s10236-011-0404-9
Tian Jiwei, Yang Qingxuan, Zhao Wei. 2009. Enhanced diapycnal mixing in the South China Sea. Journal of Physical Oceanography, 39(12): 3191–3203, doi: 10.1175/2009JPO3899.1

Umezawa Y, Yamaguchi A, Ishizaka J, et al. 2014. Seasonal shifts in the contributions of the Changjiang River and the Kuroshio Current to nitrate dynamics in the continental shelf of the northern East China Sea based on a nitrate dual isotopic composition approach. Biogeosciences, 11(4): 1297–1317, doi: 10.5194/bg-11-1297-2014

Voss M, Bombar D, Loick N, et al. 2006. Riverine influence on nitrogen fixation in the upwelling region off Vietnam, South China Sea. Geophysical Research Letters, 33(7): L07604

Wang Dakui, Wang Hui, Li Ming, et al. 2013. Role of Ekman transport versus Ekman pumping in driving summer upwelling in the South China Sea. Journal of Ocean University of China, 12(3): 355–365, doi: 10.1007/s11802-013-1904-7

Wang Daoru, Yang Yi, Wang Jia, et al. 2015. A modeling study of the effects of river runoff, tides, and surface wind-wave mixing on the eastern and western Hainan upwelling systems of the South China Sea, China. Ocean Dynamics, 65(8): 1143–1164, doi: 10.1007/s10236-015-0857-3

Wankel S D, Kendall C, Pennington J T, et al. 2007. Nitrification in the euphotic zone as evidenced by nitrate dual isotopic composition: observations from Monterey Bay, California. Global Biogeochemical Cycles, 21(2): GB2009

Weigand M A, Foriel J, Barnett B, et al. 2016. Updates to instrumentation and protocols for isotopic analysis of nitrate by the denitrifier method. Rapid Communications in Mass Spectrometry, 30(12): 1365–1383, doi: 10.1002/rcm.7570

Wong George T F, Tseng Chun-Mao, Wen Liang-Saw, et al. 2007. Nutrient dynamics and N-anomaly at the SEATS station. Deep-Sea Research Part II: Topical Studies in Oceanography, 54(14–15): 1528–1545, doi: 10.1016/j.dsr2.2007.05.011

Wu Meilin, Wang Youshao, Wang Dongxiao, et al. 2014. Effects of coastal upwelling on picophytoplankton distribution off the coast of Zhanjiang in South China Sea. Oceanological and Hydrobiological Studies, 43(3): 283–291, doi: 10.2478/s13545-014-0143-x

Wu Yunchao, Zhang Jingping, Liu Songlin, et al. 2018. Aerosol concentrations and atmospheric dry deposition fluxes of nutrients over Daya Bay, South China Sea. Marine Pollution Bulletin, 128: 106–114, doi: 10.1016/j.marpolbul.2018.01.019

Yang Jin-Yu Terence, Hsu Shih-Chieh, Dai Minhan, et al. 2014. Isotopic composition of water-soluble nitrate in bulk atmospheric deposition at Dongsha Island: sources and implications of external N supply to the northern South China Sea. Biogeosciences, 11(7): 1833–1846, doi: 10.5194/bg-11-1833-2014

You Yuzhu, Chern Ching-Sheng, Yang Yih, et al. 2005. The South China Sea, a *cul-de-sac* of North Pacific intermediate water. Journal of Oceanography, 61(3): 509–527, doi: 10.1007/s10872-005-0059-6

Zhang Run, Chen Min, Yang Qing, et al. 2015. Physical-biological coupling of N_2 fixation in the northwestern South China Sea coastal upwelling during summer. Limnology and Oceanography, 60(4): 1411–1425, doi: 10.1002/lno.10111

Zhang Jing, Wang Daoru, Jennerjahn T, et al. 2013. Land–sea interactions at the east coast of Hainan Island, South China Sea: a synthesis. Continental Shelf Research, 57: 132–142, doi: 10.1016/j.csr.2013.01.004

Zhang Liming, Wei Zhiyuan, Qi Zhiping. 2006. Characteristics of rainfall and evaporation of different region in recent 30 years in Hainan province. Chinese Agricultural Science Bulletin, 22(4): 403–407

Zhou Nan. 2020. Nutrient dynamics and nitrogen cycle in the northern South China Sea influenced by mesoscale processes [dissertation]. Qingdao: Ocean University of China

Supplementary information:

Fig. S1. Satellite images of the monthly averaged surface seawater hydrological characteristics in the northwestern South China Sea. a. Surface seawater temperature (SST) in 2015 and 2016. b. Surface seawater salinity (SSS) in 2015 and 2016. The dates were labeled in each image.

Fig. S2. Satellite images of the monthly averaged surface seawater velocity (SSV) in the northwestern South China Sea in 2015 (a) and 2016 (b). Arrows point the water flow direction and color indicates the sea water velocity. The dates were labeled in each image.

Table. S1. The *t*-test for the hydrological and biogeochemical parameters of nearshore and offshore stations of Sections A1 and A2 above 125 m in September. The nearshore stations included Stations A26 to A29 for Section A1 and Stations A30 to A33 for Section A2.

The supplementary information is available online at https://doi.org/10.1007/s13131-021-1934-8 and www.aosocean.com. The supplementary information is published as submitted, without typesetting or editing. The responsibility for scientific accuracy and content remains entirely with the authors.